Available online at www.sciencedirect.com
SCIENCE DIRECT®
Journal of Photochemistry and Photobiology A: Chemistry 163 (2004) 53–60
Journal of Photochemistry and Photobiology A:Chemistry
www.elsevier.com/locate/jphotochem

Photochemically-induced reduction and rearrangements of *N*,*N*′-bis-(carboxymethyl)-*N*,*N*′-dinitroso-1,4-phenylenediamine

Gregory Bodemer, Lara M. Ellis, Peter Jon Lace, Pamela E. Mooren, Neil K. Patel, Michael P. Ver Haag, A. Andrew Pacheco*

Department of Chemistry, University of Wisconsin-Milwaukee, 3210 North Cramer Street, Milwaukee, WI 53211, USA

Received 23 July 2003; received in revised form 25 October 2003; accepted 29 October 2003

Abstract

When irradiated with ∼10 ns laser pulses of 308 nm light, *N*,*N*′-bis-(carboxymethyl)-*N*,*N*′-dinitroso-1,4-phenylenediamine (**1**) fragments in less than a μs to give NO and the denitrosylated radical of **1** (**2**). Species **1** has great potential as a research tool because the photo-generated NO can subsequently be used to probe fast reactions of biochemical interest. This study focuses on the properties of the reactive intermediate **2**, which must be known before **1** can confidently be used in more complex investigations. Experiments in which **1** was irradiated in the presence of myoglobin (Mb) or ferrocytochrome *c* revealed that **2** can rapidly oxidize either species. For myoglobin, the rate constant k_{ox} was measured as $(5.5 \pm 0.5) \times 10^7\ M^{-1}\ s^{-1}$. Experiments in which large amounts of **2** were photo-generated in the presence of free NO revealed that **2** probably recombines with NO to produce metastable isomers of **1**, which have lifetimes of ∼20 ms and liberate additional NO as they decay. Previously, **2** was only known to either rapidly recombine with NO to regenerate **1** exclusively, or fragment further to give a second equivalent of NO and the doubly denitrosylated quinoimine derivative of **1** (**3**). The experiments with myoglobin, which is a chromophoric NO scavenger, also made it easy to quantify the amount of NO generated under various conditions, thus providing indirect information about the reactions of **2**. On the basis of these experiments, the value of the rate constant for fragmentation of **2** into **3** and NO (k_d) was revised from the previously published 500–2600 s^{-1}. The NO scavenger experiments also suggest that the metastable isomers of **1**, generated by recombination of **2** and NO, liberate additional equivalents of NO as they decay.

Keywords: *N*,*N*′-bis-(Carboxymethyl)-*N*,*N*′-dinitroso-1,4-phenylenediamine; Photochemistry; Nitric oxide synthesis; Microsecond timescale

1. Introduction

The compound *N*,*N*′-bis-(carboxymethyl)-*N*,*N*′-dinitroso-1,4-phenylenediamine (**1**) has been shown to release NO upon photo-activation with 308 nm light [1–4]. NO is now known to play numerous important roles in human physiology [5–11]. This has provided the major stimulus for synthesizing compounds such as **1**, that are biologically inert, but could potentially be activated to release NO once they reach specific biological target sites [1,3,12–14]. Though designed for such potential biomedical applications [1–3], compound **1** has also proved to be a valuable research tool for our in vitro investigations [15]. In these investigations we use the photo-generated NO as a probe for studying metalloenzyme reactions that feature, at least formally, metal-bound NO species as intermediates. NO can be generated from **1** in less than 1 μs using a XeCl excimer laser, so very fast subsequent reactions of NO with other compounds can then be monitored [1,15]. Furthermore, the concentration of NO within a given experiment is readily controlled, either by varying the intensity of the laser pulse, or by maintaining the laser pulse constant and varying the concentration of **1** [4].

Before **1** can be confidently used as a NO generator for probing the reactivity of compounds such as metalloenzymes, the amount of NO that is generated under a given set of conditions should be known as accurately as possible. Furthermore, any potential side-reactions that **1**, or products generated by its photo-fragmentation, might undergo with the metalloenzyme of interest, should be carefully investigated. A recently published paper describes how the amount of NO generated can be predicted with reasonable accuracy when solutions containing only **1** are irradiated, under conditions in which the initial photoproduct concentrations are kept below ∼10 μM [4]. More recently we have been analyzing the photochemical behavior of **1** in the presence of known NO scavenging proteins, such as myoglobin (Mb) and catalase. Herein we describe the results of these

* Corresponding author. Tel.: +1-414-229-4413; fax: +1-414-229-5530.
E-mail address: apacheco@uwm.edu (A.A. Pacheco).

1010-6030/$ – see front matter © 2004 Elsevier B.V. All rights reserved.
doi:10.1016/S1010-6030(03)00431-3

investigations. We also discuss new insights that were revealed when samples of **1**, with concentrations as high as 1 mM, were irradiated under conditions that resulted in the generation of large initial concentrations of photoproducts ($\gg$10 μM).

2. Experimental

2.1. Materials

The synthesis of the photoactive NO releasing species **1** has been described elsewhere [4]. All photochemical experiments were performed in solutions buffered with phosphate (μ = 50 mM, pH = 7.4). Millimolar stock solutions of **1** in phosphate buffer were prepared and stored in amber bottles within a glovebox. This is not essential, but proved convenient for the experiments described herein. Myoglobin (crystallized and lyophilized horse skeletal muscle) was from Sigma. Prior to use, a millimolar solution of the protein in phosphate buffer was reduced with 1 eq. of Ti(III) citrate [16], and then passed down a desalting column (Amersham Hi Trap 5 ml × 5 ml) to remove the oxidized Ti salts. All manipulations were performed in a glovebox. Twice-recrystallized bovine liver catalase (cat) was obtained from Sigma, as a suspension in water containing 0.1% thymol. Lyophilized horse heart ferricytochrome *c* (cyt c^{III}), prepared using TCA, was also obtained from Sigma. Where necessary the cyt c^{III} was reduced to ferrocytochrome *c* (cyt c^{II}) with Ti(III) citrate, then re-purified using a desalting column as described earlier for Mb. The concentrations of all Mb, cat and cyt *c* solutions were determined by UV-Vis spectroscopy [17–19].

2.2. Data collection and analysis

Photochemical fragmentation of species **1** was initiated with a 10 ns, 308 nm pulse from a XeCl excimer laser (TUI, Existar 200). An OLIS RSM-1000 spectrophotometer was used to monitor the absorbance changes induced by the laser pulse. The configuration of the laser and spectrophotometric equipment has been described in general terms elsewhere [4]. Data were collected with the OLIS RSM-1000 in one of two modes. For the experiments described in Section 3.1, in which the reactions of interest had lifetimes of less than 2 ms, the spectrophotometer was used in fixed-wavelength mode (fixed middle slit width = 0.6 mm). In this mode, the monochromator was adjusted to a desired wavelength, the reaction of interest was photo-initiated, and then the absorbance change (ΔA) at that wavelength was monitored as a function of time. A total of 1000 data points were collected at 16 μs intervals for each ΔA versus *t* trace. The complete spectra presented in Fig. 1a were constructed by collecting ΔA versus *t* traces for identical replicate solutions, at 2 nm intervals from 395 to 445 nm, and then combining these into a single three-dimensional data set. For the experiments described in Section 3.2, in which the reactions of interest had lifetimes of at least several ms, the OLIS RSM-1000 was used in rapid-scanning mode (scanning slit width = 0.2 mm). In this mode, complete spectra were collected every ms during experiments lasting a total of 30 s. For both the fixed-wavelength and rapid-scanning experiments, the monochromator entrance slitwidth was 0.6 mm, and the exit slitwidth was 0.12 mm. With one exception, all data analysis was performed using the commercially available software package Specfit/32, Version 3.0 (Spectrum Software Associates). The data presented in Fig. 2 were generated using

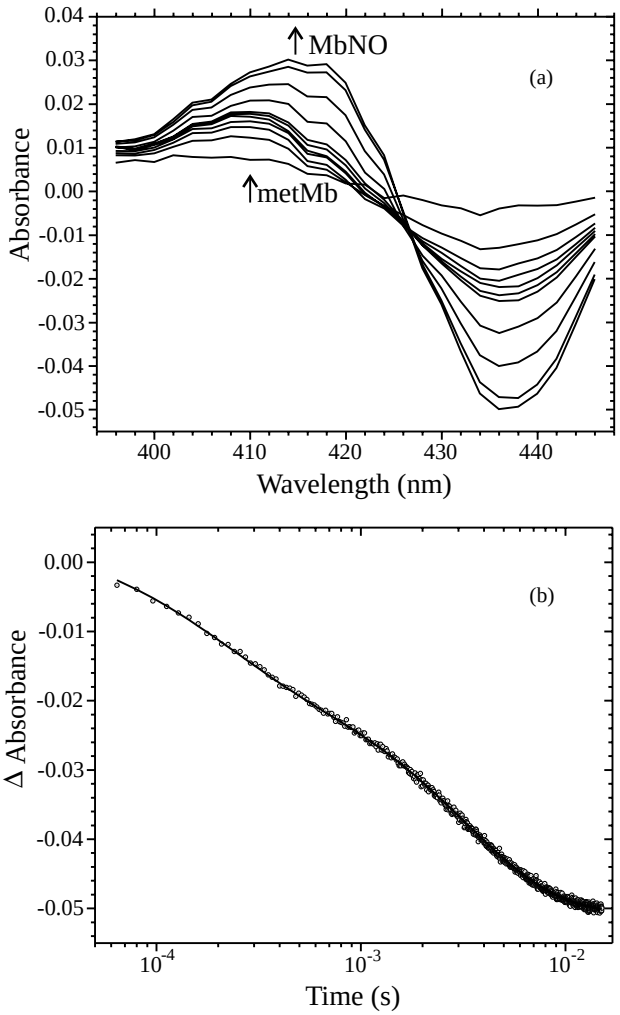

Fig. 1. (a) Spectral changes observed after a solution containing 4.04 μM **1** and 15.4 μM Mb is irradiated with a 10 ns, 308 nm laser pulse. The representative difference spectra shown here were collected 0.08, 0.24, 0.40, 0.56, 0.72, 0.88, 1, 2, 4, 8, and 15 ms after the laser flash. Initially the band growing in is centered around 410 nm, reflecting the rapid oxidation of Mb to metMb by reactive intermediate **2** (Scheme 1). After ~1 ms the band starts to red-shift, as the slower nitrosylation of Mb becomes the predominant reaction (see Section 3.1). (b) ΔA vs. time trace extracted from (a) at 436 nm. The circles are the experimental data points, collected at 16 μs intervals. The solid trace was calculated using Specfit/32, as described in Section 3.1. Comparable fits were obtained at other wavelengths.

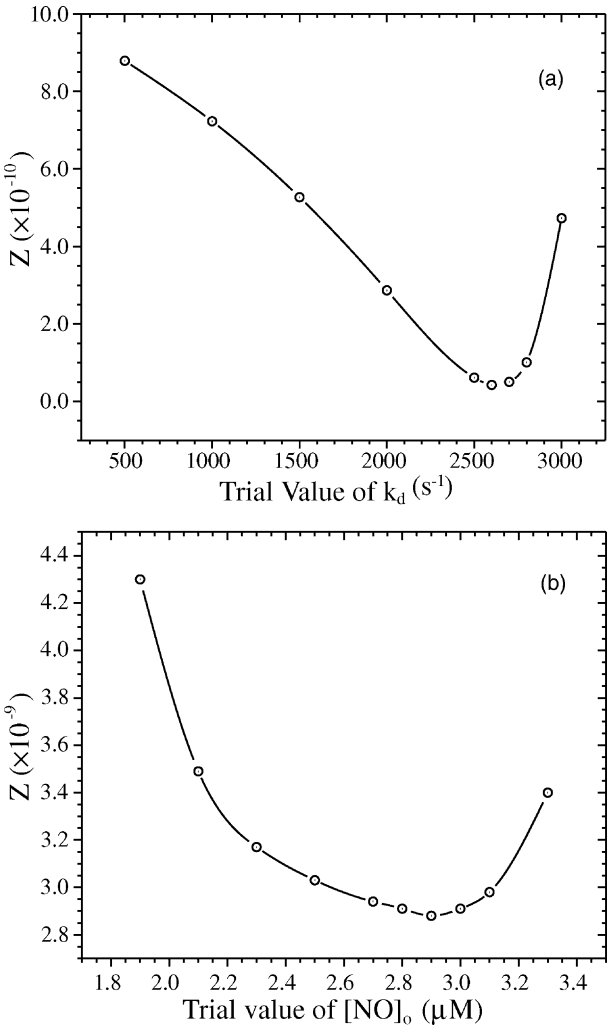

Fig. 2. (a) Plot of $Z = \sum[(\Delta\epsilon_{metMb})_{calcd} - (\Delta\epsilon_{metMb})_{exper}]^2 + \sum[(\Delta\epsilon_{MbNO})_{calcd} - (\Delta\epsilon_{MbNO})_{exper}]^2$ as a function of the trial value of k_d. $(\Delta\epsilon_{species})_{exper}$ is the difference in extinction coefficient at a given wavelength that was determined directly from pure samples of Mb, metMb and MbNO. $(\Delta\epsilon_{species})_{calcd}$ is the difference in extinction coefficient at a given wavelength that was calculated using the Specfit/32 Kinetic Model Editor, for a given value of k_d. The smallest difference between the experimentally determined difference spectra and those calculated using Specfit/32 was obtained with k_d fixed at 2600 s^{-1}. In all cases $[NO]_0$ and $[\mathbf{2}]_0$ were fixed at 1.9 μM. (b) Same as (a), but here k_d was fixed at 2600 s^{-1} in all cases, while the trial value of $[NO]_0$ (=$[\mathbf{2}]_0$) was varied. The smallest difference between the experimentally determined difference spectra and those calculated using Specfit/32 was seen with $[NO]_0$ and $[\mathbf{2}]_0$ fixed at 2.9 μM.

a simple Quick Basic (Version 4.5) routine in combination with Specfit/32.

3. Results

3.1. NO generation in the presence of myoglobin

Fig. 1a shows the UV-Vis spectral changes that are observed after irradiating a solution containing 4.04 μM **1** and 15.4 μM myoglobin (Mb) with a 308 nm laser pulse. These changes fall in the region between 400 and 450 nm, which is where heme proteins such as Mb typically exhibit a characteristic, intense absorbance band (the "Soret" band) [17,20]. The Soret band of Mb itself has a maximum value at 435 nm, right around where the major drop in absorbance is seen in Fig. 1a [17]. Hence, the observed spectral changes can be readily attributed to reactions that consume Mb to give new hemoprotein species. These species must have absorbance maxima below ~425 nm, where a net increase in absorbance is detected. The absence of isosbestic points in Fig. 1a, and the observation that ΔA_{max} for the new band shifts over time from near 410 to 415 nm, both indicate that more than one heme product is being generated as Mb is consumed. Fig. 1b shows a trace of ΔA_{436} as a function of time. The trace is clearly biphasic, with the first phase having a half life of ~800 μs, and the second ~2 ms. The shift in ΔA_{max} of the band that appears below 430 nm is associated with the second reaction phase; prior to ~1 ms this band is centered strictly at 410 nm.

Analysis of the data in Fig. 1 using singular value decomposition (SVD) reveals that two colored species are generated after the solution is irradiated. One of these species is expected to be nitrosylated Mb (MbNO), since NO is known to bind to Mb rapidly ($k_{NO} = 1.7 \times 10^7\ M^{-1}\ s^{-1}$) and very tightly [21]. Furthermore, the nitrosylation should be pseudo-first order with respect to [NO], because the [Mb] of 15.4 μM is ~ 8× greater than the ~ 2 μM [NO] expected to be generated by the laser pulse [4]. Thus, the nitrosylation phase should exhibit a half life of ~2.6 ms, which falls in the range of the second feature seen in Fig. 1b. Based on the aspects of the difference spectra prior to 1 ms, the first species generated from Mb after the laser pulse appears to be metMb, in which the Fe center has been oxidized from +2 to +3, and a water or hydroxide is bound to the metal. At pH 7.4 metMb exhibits a Soret band at 408 nm [17], whereas MbNO has an absorbance maximum at 420 nm [18].[1] The mechanism shown in Scheme 1 suggests how both MbNO and metMb could be generated from Mb, following irradiation of the reaction mixture with 308 nm light. The first two steps of Scheme 1 are the reactions proposed by Namiki et al. for solutions containing only **1** [1]. The initial laser flash causes the fragmentation of **1** into 1 eq. of NO and the radical species **2** (Step 1). Species **2** can recombine with NO to give back the starting compound **1**, or it can fragment further to give a second equivalent of NO and species **3** (Step 2). In the absence of the intensely colored heme species the generation and subsequent disappearance of **2** can be readily monitored by UV-Vis spectroscopy, since **2** has a characteristic band with λ_{max} −400 nm [1,4]. In the presence of Mb a new reaction path appears to open for species **2**: it can now

[1] metMb itself also reacts with NO. However, the binding constant for the reaction is low ($1.4 \times 10^4\ M^{-1}$), and the reaction is 100× slower than Mb + NO (refs: [18,21]). Hence, this reaction is not expected to play a significant role in the system discussed here.

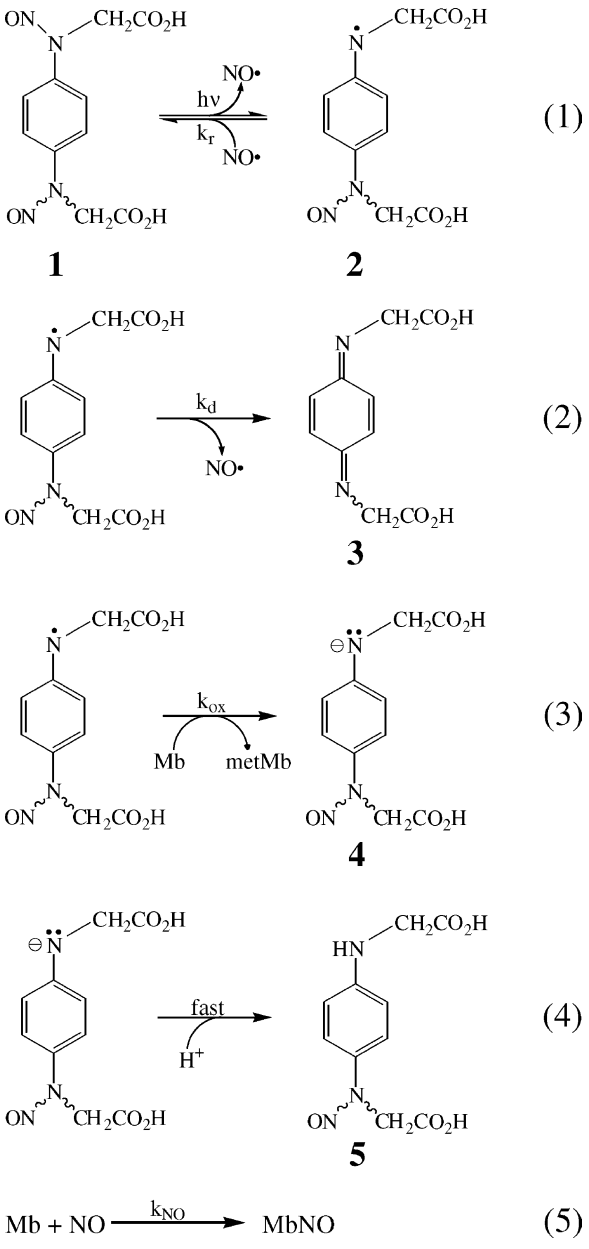

Scheme 1.

be reduced to **4** by the Mb, which is concomitantly oxidized to metMb (Step 3). Species **4** is probably then protonated to give species **5** (Step 4), though we have no information about the pK_a of **5** at this time. Finally, all of the NO that is generated in Steps 1 and 2 but does not recombine with **2** will eventually be scavenged by Mb to give MbNO (Step 5).

The data of Fig. 1 were analyzed on the basis of the mechanism shown in Scheme 1, using the Specfit/32 Kinetic Model Editor (see Section 2.2). Initially the values for k_r and k_d were fixed at $1 \times 10^9\,M^{-1}\,s^{-1}$ and $500\,s^{-1}$, respectively, which are values previously obtained in independent experiments [4]. Similarly, the concentrations of NO and **2** present immediately after the laser flash ($[NO]_0$ and $[\mathbf{2}]_0$) were fixed at 1.9 μM, the value predicted on the basis of our previous investigations [4]. Only k_{ox} and k_{NO} were left as adjustable parameters, to be determined by the Specfit/32 program. This analysis gave excellent least-square fits to the experimental ΔA versus t traces at all wavelengths (comparable to the fit seen in Fig. 1b). Moreover, the calculated value of k_{NO} was comparable to the $1.7 \times 10^7\,M^{-1}\,s^{-1}$ value previously reported by Hoshino et al. [21]. However, the difference spectra $\epsilon_{MbNO} - \epsilon_{Mb}$ ($\equiv \Delta\epsilon_{MbNO})_{calcd}$ and $\epsilon_{metMb} - \epsilon_{Mb}$ ($\equiv \Delta\epsilon_{metMb})_{calcd}$ that were calculated on the basis of this analysis compared poorly with the difference spectra $(\Delta\epsilon_{MbNO})_{exper}$ and $(\Delta\epsilon_{metMb})_{exper}$ obtained independently from pure samples of Mb, MbNO and metMb. $|\Delta\epsilon_{metMb}|_{calcd}$ was about 3× smaller than expected at every wavelength, whereas $|\Delta\epsilon_{MbNO}|_{calcd}$ was somewhat larger than expected. In order to obtain better agreement between the calculated and the experimentally obtained difference spectra, the following iterative procedure was used. First, the experimental data were fitted repeatedly using Specfit/32 as described above, but using different fixed k_d values each time. Agreement between the calculated and experimental $\Delta\epsilon_{metMb}$ spectra became progressively better as the trial value of k_d was increased from 500 to $2600\,s^{-1}$, and then became poorer again for trial values of k_d greater than $2600\,s^{-1}$. This is seen in Fig. 2a, which is a plot of $\sum[(\Delta\epsilon_{metMb})_{calcd} - (\Delta\epsilon_{metMb})_{exper}]^2 + \sum[(\Delta\epsilon_{MbNO})_{calcd} - (\Delta\epsilon_{MbNO})_{exper}]^2$ (abbreviated as Z) as a function of the trial value of k_d. Although Z contains the least-squares expressions for both MbNO and metMb, $(\Delta\epsilon_{MbNO})_{calcd}$ was not noticeably affected by varying the trial value of k_d.

In the next phase the experimental data were repeatedly fitted with k_d fixed at the new best value of $2600\,s^{-1}$, but using different values of $[NO]_0$ (=$[\mathbf{2}]_0$) each time. This procedure gave progressively better agreement between $(\Delta\epsilon_{MbNO})_{calcd}$ and $(\Delta\epsilon_{MbNO})_{exper}$ as the trial values of $[NO]_0$ and $[\mathbf{2}]_0$ were increased from 1.9 to 2.9 μM, after which the agreement became worse again. Varying the trial values of $[NO]_0$ and $[\mathbf{2}]_0$ had no noticeable effect on $(\Delta\epsilon_{metMb})_{calcd}$. Fig. 2b shows a plot of the trial statistic Z as a function of trial $[NO]_0$ and $[\mathbf{2}]_0$. Fig. 3 shows the comparisons between experimental and calculated difference spectra $\Delta\epsilon_{metMb}$ and $\Delta\epsilon_{MbNO}$, obtained using the adjusted values of k_d and $[NO]_0$ (=$[\mathbf{2}]_0$). The corresponding values of k_{ox} and k_{NO} that were calculated by the Specfit/32 program were $(5.5 \pm 0.5) \times 10^7$ and $(2.20 \pm 0.01) \times 10^7\,M^{-1}\,s^{-1}$, respectively. The latter value is close to that previously reported by Hoshino et al. [18]. The theoretical ΔA_{436} versus t trace of Fig. 1b was obtained using these values of k_{ox} and k_{NO}.

In addition to Mb, **2** was found to readily oxidize cyt c^{II} to cyt c^{III} (results not shown), even though the cyt c^{III}/cyt c^{II} standard reduction potential is 214 mV higher than that of metMb/Mb [22,23]. Cyt c^{III} does not react either with **2** or with NO on the sub-second timescale. When **1** was photolyzed in the presence of cat, catNO was the only detected reaction product. Like Mb, cat is known to bind NO rapidly and tightly [18]. However, it appears that **2** is not ca-

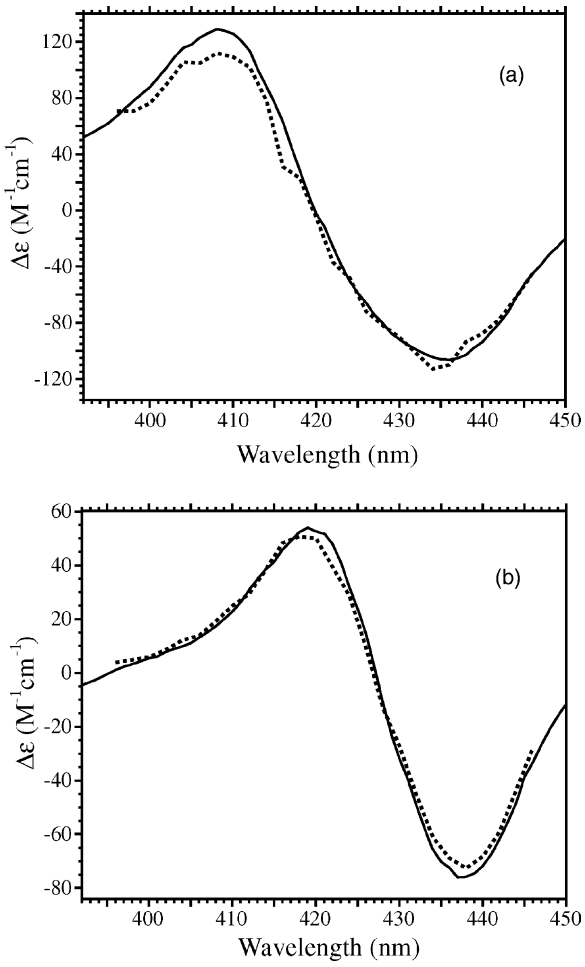

Fig. 3. (a) Difference spectra for (metMb–Mb). Solid line: $(\Delta\epsilon_{metMb})_{exper}$; dotted line: $(\Delta\epsilon_{metMb})_{calcd}$. (b) Difference spectra for (MbNO–Mb). Solid line: $(\Delta\epsilon_{MbNO})_{exper}$; dotted line: $(\Delta\epsilon_{MbNO})_{calcd}$. The parameters associated with the calculated spectra were: $k_r = 1 \times 10^9\,M^{-1}\,s^{-1}$; $k_d = 2600\,s^{-1}$; $k_{ox} = (5.5 \pm 0.5) \times 10^7\,M^{-1}\,s^{-1}$; $k_{NO} = (2.20 \pm 0.01) \times 10^7\,M^{-1}\,s^{-1}$; $[NO]_0 = [\mathbf{2}]_0 = 2.9\,\mu M$.

pable of oxidizing the Fe^{III} heme centers of the cat resting enzyme.

3.2. Photolysis of concentrated samples of *1*

In solutions that contain only **1** to start with, the mechanism of Scheme 1 allows only two fates for the photogenerated species **2**: it can recombine with NO, or it can further fragment to give species **3** and a second equivalent of NO [1,4]. Thus, Scheme 1 predicts that an irradiated solution of **1** should contain only **1** and **3** after all of the photogenerated species **2** has reacted (i.e.: after at most ∼2 ms [4]). Early studies showed that species **3** (Scheme 1) has no significant absorbance in the visible region [1], and hence the final difference spectrum should be flat, except for a small negative feature below 400 nm due to the conversion of **1** (with $\lambda_{max} = 300$ nm) to **3**. This prediction based on Scheme 1 proves to be essentially correct under conditions

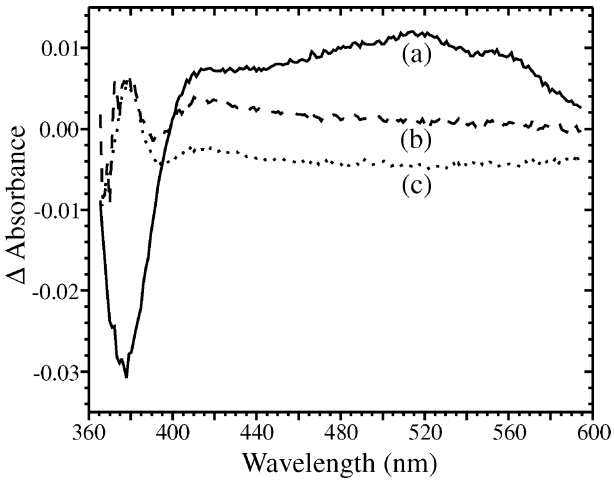

Fig. 4. (a) Difference spectrum obtained 1 ms after irradiating a solution, containing 1.21 mM of **1** and 0.676 mM free NO, with a 308 nm laser pulse. Note the prominent broad band at ∼515 nm. (b) Same solution as (a) but 1 s after the laser pulse. (c) Same solution after 30 s.

in which less than 10 μM of **2** is initially generated by the laser pulse [1,4]. However, we have found that it is *not* true under conditions in which comparatively large amounts of **2** are generated by the initial photolysis of **1**.

When solutions of **1** with concentrations greater than 20 μM are irradiated with full intensity laser pulses, using the laser apparatus described in Section 2, the UV-Vis difference spectra of the samples after several ms exhibit positive deflections in ΔA at all wavelengths between ∼400 and 580 nm (Fig. 4a). These difference spectra are quite distinct from that of species **2** [1], which in any case is consumed on the μs timescale. Of key importance is the fact that the positive ΔA is observed even in solutions containing an excess of free NO. Indeed, ΔA is undiminished regardless of the free [NO]. Trace (a) in Fig. 4 gives the example of a UV-Vis difference spectrum collected 1 ms after irradiating a solution containing 1.21 mM of **1** and 0.676 M of free NO with a 308 nm laser pulse. The spectrum exhibits a broad positive deflection band with $\lambda_{max} \sim 515$ nm, and a sharper negative deflection band centered at ∼380 nm. Based on Scheme 1 and the previously calculated values of k_r and k_d (this work and refs. [1,4]), under the conditions in which the spectrum was collected *all* of the photogenerated intermediate **2** should have been converted back to **1** in less than 1 μs.

The spectrum shown in Fig. 4a proves to be transient, and after ∼ 1 s the band at 515 nm disappears completely. SVD analysis of spectra collected every ms for 30 s following laser irradiation shows that changes in these can be roughly modeled on the basis of a three-component system, in which each component decays to the next in a first-order process. Traces (b) and (c) in Fig. 4 show the spectra obtained after 1 s and 30 s, respectively, while Fig. 5 shows the ΔA versus t trace obtained at 515 nm, empirically fitted to two exponentials. The rate constant for the first exponential phase in Fig. 5 is $36.5 \pm 0.2\,s^{-1}$ ($t_{0.5} = 19$ ms), while that of the second is $(8.8 \pm 0.4) \times 10^{-2}\,s^{-1}$ ($t_{0.5} = 7.9$ s). A series of

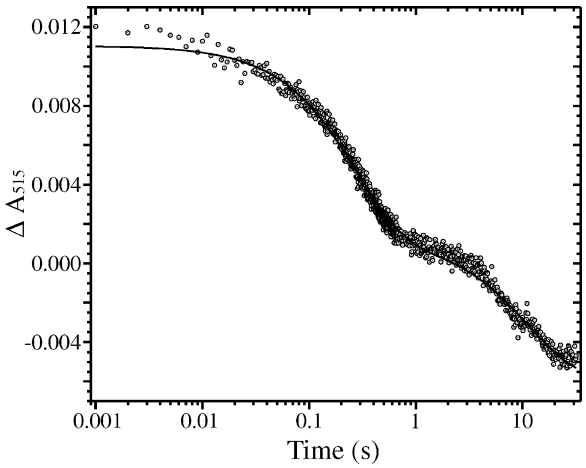

Fig. 5. ΔA vs. time trace extracted from Fig. 4 at 515 nm. The circles are the experimental data points, collected at 1 ms intervals. The solid trace was calculated using Specfit/32, as described in Section 3.2. Comparable fits were obtained at other wavelengths.

experiments in which [NO] was varied revealed that the first reaction phase is independent of [NO]. The rate constant of the second phase, however, varied in an unpredictable way from one experiment to the next. This phase is probably due primarily to physical transport of reactants and products, via diffusion and convection, into and out of the region of the cuvette that was irradiated by the laser pulse. Variations in the quiescence of the solutions from one experiment to the next could account for the observed variability of the rate constant.

Scheme 2 suggests modifications to the currently accepted mechanism that could explain both the presence of spectral features in Fig. 4a, and why these features disappear in the first exponential phase (Fig. 5). It has previously been assumed that recombination of NO with **2** would give back **1** exclusively [1,4]. However, as seen in Scheme 2, the radical intermediate **2** should formally be described in terms of three resonance structures, **2**, **2a** and **2b**. If there is indeed significant spin delocalization from the nitrogen to the *o* and *p* carbons of the intermediate, then the incoming NO could re-attach at either of these carbons, to give **6** or **7** instead of **1**. These two species would then together be responsible for the spectral features of Fig. 4a. The comparatively low intensity of the spectral features would explain why they were not detected in earlier experiments, in which only small amounts of **6** and **7** would have been generated [1,4].

One can envision several pathways by which the putative species **6** and **7** could react, and thus give rise to the decrease in ΔA that is observed over the ms timescale. For example, both **6** and **7** would be expected to readily re-release NO and form **2** again. This would provide a pathway by which most of the compound **1** lost in the initial photo-dissociation would eventually be recovered, albeit on a timescale dominated by the rate constants k_{-r2} and k_{-r3}, not by k_{r1} (Scheme 2). Putative species **6** also has an additional reaction pathway available to it that is not available to **7**, and that is tautomerization to give species **8** (Scheme 2). The three rate constants, k_{-r2}, k_{-r3} and k_{taut}, would together contribute to the apparent first-order rate constant observed for the decay of the 515 nm feature in Fig. 4a. The availability of a tautomerization pathway that produces a stable species (**8**) could explain why even spectra b and c are not featureless.

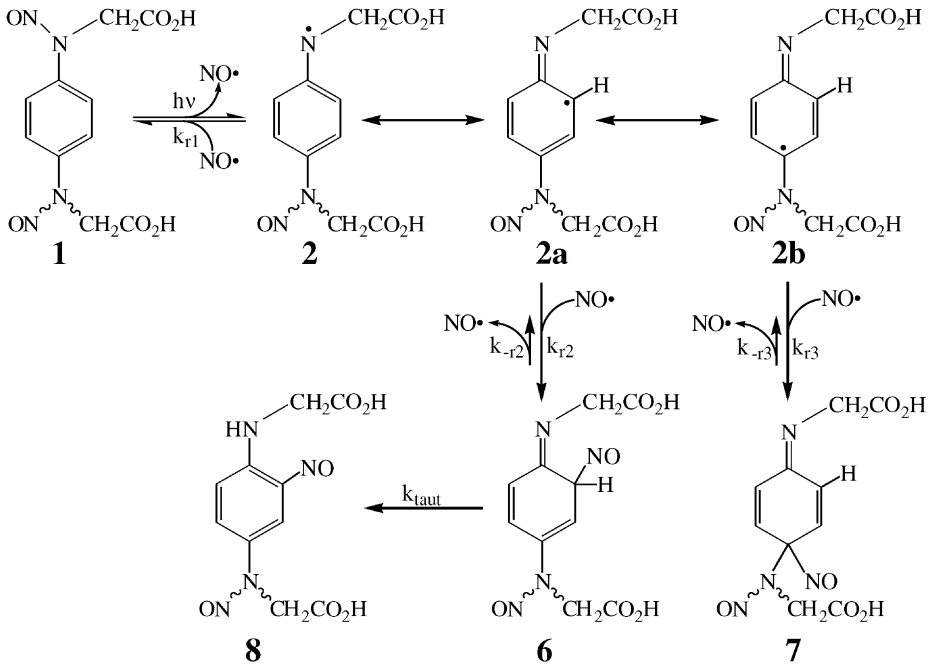

Scheme 2.

4. Discussion

The results presented in Section 3.1 clearly demonstrate that intermediate **2** is a reasonably powerful oxidant (Scheme 1). Those presented in Section 3.2 suggest a second previously unreported property of **2**, namely that it can react with NO to give isomers other than **1** (Scheme 2). These new observations are potentially of great practical importance for the design of experiments that use **1** as a NO generator.

If the species to be nitrosylated is also a reducing agent, then one must keep in mind that it may react with **2** in the same way as Mb does (Step 3, Scheme 1), in addition to reacting with NO. While the oxidizing properties of **2** undoubtedly increase the complexity of the system, they could conceivably be exploited by clever experimental design. The reduction of species **2** to give **4** (Step 3, Scheme 1) competes with its nitrosylation by free NO to generate **1** and its isomers (Step 1, Scheme 1, and Scheme 2). Because the reduction of **2** is ultimately irreversible (at least under the conditions used in our experiments), this reaction provides a method for permanently removing **2** without decreasing the overall concentration of free NO that will be left after all of **2** has reacted. Reduction of **2** is second order overall, so the reaction rate can be increased by increasing the concentration of reductant. Thus, in principle, fairly high concentrations of free NO could be trapped by deliberately adding large concentrations of a suitable reducing agent to the reaction mixture. The reductant could be either the species being nitrosylated, or a separate reagent added for the specific purpose of scavenging **2**. In the absence of a reducing agent, the only pathway whereby free NO can be trapped for the long term is Step 2, Scheme 1, in which a second equivalent of NO dissociates from **2** to generate the stable quinoimine derivative **3** [1,4]. This reaction is first-order overall, and thus cannot compete effectively with the recombination of NO and **2**, when these species are present in high concentrations. As a consequence the amount of free NO that can be generated in the absence of a reducing agent is inherently limited [4].

The fact that **2** may be capable of reacting with NO to give isomers other than **1** (Scheme 2, Section 3.2) will also have to be taken into account when designing experiments that use **1** as a source of NO for a subsequent nitrosylation reaction. According to the results described in Section 3.2, and the interpretation presented in Scheme 2, species **6** and **7** are expected to release NO during a period of ∼1 s after the initial laser flash. Thus, the amount of NO ultimately available for nitrosylation reactions will be higher (possibly considerably higher) than the amount of free NO remaining after the concentration of species **2** has been reduced to negligible levels. If the nitrosylation reaction of interest is very fast compared to the dissociation of NO from **6** and **7** ($t_{0.5} \ll 20$ ms), then nitrosylation by free NO will appear as a rapid phase, clearly distinguishable from later nitrosylation by NO released as **6** and **7** fragment. Such behavior is indeed observed when Mb and cat are nitrosylated under conditions that initially generate large amounts of **2** (data not shown). Quantitative analyses of such reactions are currently under way in our laboratories. For very slow nitrosylations kinetic analysis should also be straightforward. Such reactions will have proceeded very little by the time **6** and **7** have been completely consumed, and so only a single kinetic phase will be observed, corresponding to the reaction of the species of interest with whatever concentration of free NO is then available. If the nitrosylation reaction of interest has a rate comparable to the rate of dissociation of NO from **6** and **7**, then nitrosylation by free NO and by NO released from decomposition of **6** and **7** will overlap, making kinetic analysis complicated. Species **1** will likely be least useful as a NO generator for investigating these types of reactions.

In summary, when designing future experiments that use **1** as a photo-activated NO generator, two new factors should be considered. Firstly the oxidizing properties of species **2**, the fragmentation product of **1**, must be taken into account. Secondly, **2** appears to recombine with free NO to give metastable isomers other than **1**. Spectroscopic and theoretical investigations of these putative metastable isomers are currently under way in our laboratories.

Acknowledgements

This work was supported with funds from the University of Wisconsin-Milwaukee Graduate School.

References

[1] S. Namiki, T. Arai, K. Fujimori, J. Am. Chem. Soc. 119 (1997) 3840–3841.
[2] S. Namiki, F. Kaneda, M. Ikegami, T. Arai, K. Fujimori, S. Asada, H. Hama, Y. Kasuya, K. Goto, Bioorg. Med. Chem. 7 (1999) 1695–1702.
[3] M. Yoshida, I. Masashi, S. Namiki, T. Arai, K. Fujimori, Chem. Lett. (2000) 730–731.
[4] M.Z. Cabail, P.J. Lace, J. Uselding, A.A. Pacheco, J. Photochem. Photobiol. A: Chem. 152 (2002) 109–121.
[5] J.B. Hibbs, Z. Vavrin, R.R. Taintor, J. Immunol. 138 (1987) 550–565.
[6] S. Moncada, R.M.J. Palmer, E.A. Higgs, Biochem. Pharmacol. 38 (1989) 1709–1715.
[7] H. Bult, G.E. Boeckxstaens, P.A. Pelckmans, F.H. Jordaens, Y.M. Van Maercke, A.G. Herman, Nature 345 (1990) 346–347.
[8] K. Shibuki, D. Okada, Nature 349 (1991) 326–328.
[9] D.S. Bredt, P.M. Hwang, C.E. Glatt, C. Lowenstein, R.R. Reed, S.H. Snyder, Nature 351 (1991) 714–718.
[10] D.E. Heck, D.L. Laskin, C.R. Gardner, J.D. Laskin, J. Biol. Chem. 267 (1992) 21277–21280.
[11] P.C. Ford, I.M. Lorkovic, Chem. Rev. 102 (2002) 993–1017.
[12] J. Bourassa, W. DeGraff, S. Kudo, D.A. Wink, J.B. Mitchell, P.C. Ford, J. Am. Chem. Soc. 119 (1997) 2853–2860.
[13] M. De Leo, P.C. Ford, J. Am. Chem. Soc. 121 (1999) 1980–1981.
[14] Y. Hou, W. Xie, A.J. Janczuk, P.G. Wang, J. Org. Chem. 65 (2000) 4333–4337.

[15] M.Z. Cabail, A.A. Pacheco, Inorg. Chem. 42 (2003) 270–272.
[16] R. Codd, A.V. Astashkin, A. Pacheco, A.M. Raitsimring, J.H. Enemark, J. Biol. Inorg. Chem. 7 (2002) 338–350.
[17] B.R. James, Physical chemistry, in: D. Dolphin (Ed.), The Porphyrins, vol. V, Part C, Academic Press, New York, 1978, pp. 207–302.
[18] M. Hoshino, K. Ozawa, H. Seki, P.C. Ford, J. Am. Chem. Soc. 115 (1993) 9568–9575.
[19] E. Margoliash, N. Frohwirt, Biochem. J. 71 (1959) 570–573.
[20] M. Gouterman, Physical chemistry, in: D. Dolphin (Ed.), The Porphyrins, vol. III, Part A, Academic Press, New York, 1978, pp. 1–158.
[21] M. Hoshino, M. Maeda, R. Konishi, H. Seki, P.C. Ford, J. Am. Chem. Soc. 118 (1996) 5702–5707.
[22] H.B. Gray, W.R. Ellis, in: I. Bertini, H.B. Gray, S.J. Lippard, J.S. Valentine (Eds.), Bioinorganic Chemistry, University Science Books, Mill Valley, CA, 1994, p. 354.
[23] K. Shikama, Chem. Rev. 98 (1998) 1357–1373.